



# Nitrogen fixation rates in the Guinea Dome and the equatorial upwelling regions in the Atlantic Ocean

Ana Fernández-Carrera · Rainer Kiko · Helena Hauss · Douglas S. Hamilton · Eric P. Achterberg · Joseph P. Montoya · Marcus Dengler · Peter Brandt · Ajit Subramaniam

Received: 28 November 2022 / Accepted: 26 September 2023  
© The Author(s) 2023

**Abstract** Biological nitrogen fixation is a key process balancing the loss of combined nitrogen in the marine nitrogen cycle. Its relevance in upwelling or high nutrient regions is still unclear, with the few available studies in these regions of the ocean reporting rates that vary widely from below detection limit to  $> 100 \text{ nmol N L}^{-1} \text{ d}^{-1}$ . In the eastern tropical Atlantic Ocean, two open ocean upwelling systems are active in boreal summer. One is the seasonal equatorial upwelling, where the residual phosphorus associated with aged upwelled waters is suggested to enhance nitrogen fixation in this season. The other

is the Guinea Dome, a thermal upwelling dome. We conducted two surveys along  $23^\circ \text{ W}$  across the Guinea Dome and the Equator from  $15^\circ \text{ N}$  to  $5^\circ \text{ S}$  in September 2015 and August–September 2016 with high latitudinal resolution (20–60 nm between stations). The abundance of *Trichodesmium* colonies was characterized by an Underwater Vision Profiler 5 and the total biological nitrogen fixation in the euphotic layer was measured using the  $^{15}\text{N}_2$  technique. The highest abundances of *Trichodesmium* colonies were found in the area of the Guinea Dome ( $9^\circ$ – $15^\circ \text{ N}$ ) with a maximum of 3 colonies  $\text{L}^{-1}$  near the surface. By contrast, colonies were almost absent in the Equatorial band between  $2^\circ \text{ N}$  and  $5^\circ \text{ S}$ . The highest nitrogen fixation rate was measured at the northern edge

**Supplementary Information** The online version contains supplementary material available at <https://doi.org/10.1007/s10533-023-01089-w>.

A. Fernández-Carrera (✉)  
Department of Biological Oceanography, Leibniz-Institute for Baltic Sea Research Warnemuende, 18119 Rostock, Germany  
e-mail: ana.carrera@io-warnemuende.de

R. Kiko · H. Hauss · E. P. Achterberg · M. Dengler · P. Brandt  
GEOMAR Helmholtz Centre for Ocean Research Kiel, 24148 Kiel, Germany

R. Kiko  
Laboratoire d’Océanographie de Villefranche-sur-Mer, 06230 Villefranche-sur-Mer, France

H. Hauss  
Norwegian Research Centre AS (NORCE), 4021 Stavanger, Norway

D. S. Hamilton  
Department of Marine, Earth, and Atmospheric Science, NC State University, Raleigh, NC 27695, USA

J. P. Montoya  
School of Biological Sciences, Georgia Institute of Technology, Atlanta, GA 30332, USA

P. Brandt  
Faculty of Mathematics and Natural Sciences, Kiel University, 24118 Kiel, Germany

A. Subramaniam  
Lamont-Doherty Earth Observatory, Columbia University, Palisades, NY 10964, USA

of the Guinea Dome in 2016 (ca. 31 nmol N L<sup>-1</sup> d<sup>-1</sup>). In this region, where diazotrophs thrived on a sufficient supply of both phosphorus and iron, a patchy distribution was unveiled by our increased spatial resolution scheme. In the Equatorial band, rates were considerably lower, ranging from below detection limit to ca. 4 nmol N L<sup>-1</sup> d<sup>-1</sup>, with a clear difference in magnitude between 2015 (rates close to zero) and 2016 (average rates around 2 nmol N L<sup>-1</sup> d<sup>-1</sup>). This difference seemed triggered by a contrasting supply of phosphorus between years. Our study stresses the importance of surveys with sampling at fine-scale spatial resolution, and shows unexpected high variability in the rates of nitrogen fixation in the Guinea Dome, a region where diazotrophy is a significant process supplying new nitrogen into the euphotic layer.

**Keywords** Biological nitrogen fixation · Equatorial Atlantic · Guinea Dome · Thermal domes · Upwelling systems · Nutrients · Diazotrophs

## Introduction

The availability of combined nitrogen (i.e., those forms of nitrogen covalently bonded to one or more elements other than nitrogen) controls primary productivity by phytoplankton in most marine systems (Vitousek and Howarth 1991). Even though, nitrogen undergoes a complex biogeochemical cycle, involving many different biologically-mediated transformations between oxidation states (Gruber 2008; Capone and Hutchins 2013), on a global scale its bioavailability in the oceans is mainly determined by the balance of two biological processes: loss through denitrification and gain through nitrogen fixation (Gruber 2004; Zehr and Capone 2020). Nitrogen fixation is therefore the only process mediated by marine organisms that actually supplies new combined nitrogen to the upper ocean. The different approaches applied for constraining the annual contribution of this process to the nitrogen cycle in the global ocean (e.g., biogeochemical tracers, models, in situ measurements) yield a wide range between 5 and 303 Tg N year<sup>-1</sup>, mostly due to the extremely different global distribution patterns predicted by each of them (Table 2 in Tang et al. 2019a). These discrepancies might be a consequence of the many unresolved uncertainties in the ecology

and controlling factors of the nitrogen fixers (Zehr and Bombar 2015; Landolfi et al. 2018), and/or the scarcity of high-resolution studies for understanding the effect of mesoscale and submesoscale features and bridging the gap between small-scale observations towards global estimates (Benavides and Robidart 2020). All this makes modeling the nitrogen cycle a challenging task. In addition, the number of in situ measurements for validation of the models is limited, based on different methodologies and with low spatial and temporal resolutions, for instance, there was about 1110 stations in the world's ocean measured over the last 60 years according to the database in Tang et al. (2019b), which was recently updated by Shao et al. (2023) to almost 3000. In spite of all the extensive efforts to date, we still need studies combining different approaches for defining the ecophysiology of nitrogen fixers in order to constrain this flux (Zehr and Bombar 2015). In our opinion, quantifying nitrogen fixation rates and the consequent supply of new nitrogen to the euphotic zone is also essential to our understanding of the biological carbon pump and carbon sequestration.

Nitrogen fixation is an energetically expensive metabolic process that was traditionally suggested to be negligible in upwelling systems, where combined nitrogen is readily available, and therefore it was disregarded in nutrient-replete systems for a long time (Karl et al. 2002). The few available studies in upwelling regions of the ocean report a high variability of this process, ranging from below detection limit to as high as ca. 127 nmol N L<sup>-1</sup> d<sup>-1</sup> (Benavides et al. 2011; Sohm et al. 2011; Subramaniam et al. 2013; Wasmund et al. 2015; Fernandez et al. 2015; Moreira-Coello et al. 2017; Wen et al. 2017; Mills et al. 2020). In the eastern tropical Atlantic Ocean, two open ocean upwelling systems are active in boreal summer: the seasonal equatorial upwelling and the Guinea Dome. The equatorial upwelling develops in early to mid summer, lowering surface ocean temperatures by about 6 °C (Hummels et al. 2014). It is discernible by satellite imagery as a tongue of cold water with enhanced primary productivity extending from the west coast of central Africa to ca. 35° W (Grotsky et al. 2008). The residual phosphorus supply associated with aged upwelled waters, that is, the phosphorus that is still available after the concurrently upwelled nitrogen is exhausted by phytoplankton, was suggested

to enhance nitrogen fixation in this season (Subramaniam et al. 2013) relative to the boreal spring or fall (Shao et al. 2023). The Guinea Dome is a thermal upwelling dome in the northeastern tropical Atlantic with a cyclonic circulation composed of the eastward North Equatorial Countercurrent to the south and the westward North Equatorial Current to the north (Doi et al. 2009). The center of the Guinea Dome shifts seasonally between 9° and 11° N and between 22° and 25° W over horizontal scales of 700–1000 km, with upward displacements of the thermocline and pycnocline of typically 30–80 m in the upper 350 m of the ocean (Siedler et al. 1992). The 20 °C isotherm is often as shallow as 20 m with concomitant elevated nutriclines and enhanced productivity. The Guinea Dome develops in late spring to late fall in the area of the oxygen minimum zone of the tropical North Atlantic Ocean (Doi et al. 2009; Brandt et al. 2015). Additionally, ocean–atmosphere interactions in this region on time scales of a few days enhance vertical nutrient fluxes in the upper thermocline during boreal summer and early fall (Hummels et al. 2020). The Dome is located downwind of the Sahara Desert and the atmospheric deposition of iron contained within dust aerosols would suffice to fully support nitrogen fixers (Berman-Frank et al. 2001; Mahaffey et al. 2003; Rijkenberg et al. 2012; Ibánhez et al. 2022). The scarce and sparse information on the variability of nitrogen fixation in this region is usually included into the eastern tropical North Atlantic biogeochemical province (Longhurst 1995), disregarding the particularities of the Guinea Dome. Nitrogen fixation values reported in this region range from below detection limit to almost 70 nmol N L<sup>-1</sup> d<sup>-1</sup> (Voss et al. 2004; Grosskopf et al. 2012; Singh et al. 2017).

Here, we present nitrogen fixation rates obtained at a relatively high spatial resolution along 23° W at the end of boreal summer in 2015 and 2016. The hypothesis driving our study was that the low N:P ratio waters, resulting from residual phosphorus in aged upwelled waters, enhances nitrogen fixation relative to other seasons in the Guinea Dome and the Equatorial Atlantic. In addition, we expected that our fine-scale spatial resolution measurements would uncover spatial patterns in nitrogen fixation rates that are not discernable in the traditional sampling scheme of large scale oceanographic cruises (Rees et al. 2015;

Sloyan et al. 2019) where stations are often 200 nm (3–4 degrees of latitude) apart.

## Methods

### Sampling and hydrography

We conducted two surveys in the central Atlantic Ocean along 23° W from ca. 15° N to ca. 5° S in the periods between 8 September–13 October 2015 and 28 August–3 October 2016. The cruises were part of the German Collaborative Research Center 754 (SFB 754) for studying the coupling of tropical climate variability and circulation with the ocean's oxygen and nutrient balance (Krahmann et al. 2021). Here, we describe the contribution of biological nitrogen fixation in the euphotic layer along 23° W with a focus on two regions with shallow depths of the deep chlorophyll maximum in the Guinea Dome and at the Equator.

Hydrographic data were collected on a regular grid of stations with a separation of 30 min of latitude (30 nm, equivalent to ca. 56 km) between 15°–2° N and 2°–5° S, and 20 min of latitude (20 nm, equivalent to ca. 37 km) between 2° N–2° S (Hahn et al. 2017). Temperature, salinity, and chlorophyll *a* fluorescence were measured with a SeaBird SBE11 plus equipped with Conductivity-Temperature-Depth (CTD) sensors and a Wet Labs ECO-AFL/FL fluorometer. It was attached to a rosette containing 20 Niskin bottles of 10 L (Krahmann 2016; Dengler and Krahmann 2019). The depth of the mixed layer was estimated using the density profiles of the CTD and the approximation to a relatively uniform region of density proposed by Kara et al. (2000) using a variation of 0.125 kg m<sup>-3</sup> as the threshold value in the function within the *rcalcofi* package in R (Weber and McClatchie 2009).

Velocity data were continuously recorded by a 75-kHz vessel-mounted Acoustic Doppler Current Profiler (ADCP) along the section (Brandt et al. 2017; Dengler et al. 2019). The accuracy of 1-h averaged ADCP velocity data was better than 2–4 cm s<sup>-1</sup> (Fischer et al. 2003). Zonal velocities were used for defining the position and strength of different zonal currents in the region.

In 2015, our sampling began on September 8th at the Cape Verde Ocean Observatory time series

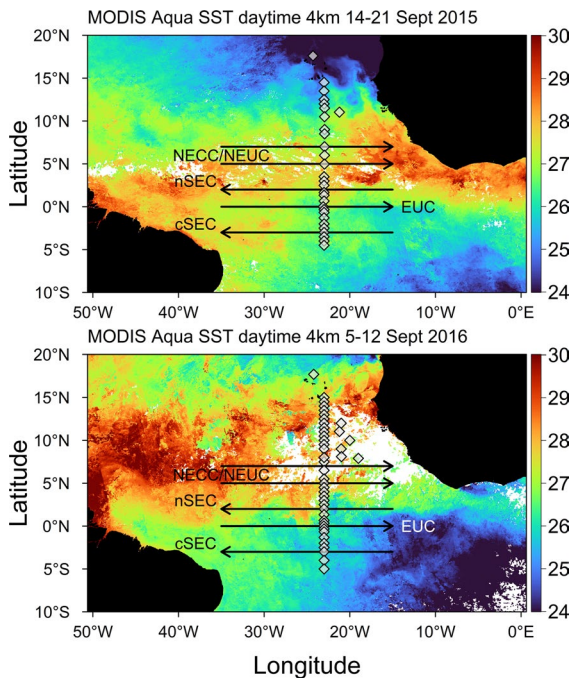


**Fig. 1** MODIS Aqua Sea Surface Temperature (day time, 4 km, 8-day composite) maps for 14–21 September 2015 (top) and 5–12 September 2016 (bottom). The sampling locations are shown as diamonds. Arrows represent a schematic of the average position of the major zonal currents crossing the 23° W meridian: North Equatorial Countercurrent (NECC), North Equatorial Undercurrent (NEUC), northern branch of the South Equatorial Current (nSEC), Equatorial Undercurrent (EUC), and central branch of the South Equatorial Current (cSEC)

(CVOO, <http://cvo0.geomar.de/>) at 17.6° N 24.3° W and finished on September 26th at a station at 4.5° S 23° W (Fig. 1). During this cruise, we also did an additional station east of the transect at 11.0° N 21.2° W associated with a deep mooring in the Guinea Dome. In 2016, the first station took place on 30th August at the CVOO, the last station was on September 18th at 5° S 23° W, and we sampled six additional stations in the area where the core of the Guinea Dome is expected between 12°–8° N and 19°–21° W, including the location of the deep mooring mentioned above (Fig. 1).

## Nutrients

In 2015, between five and seven depths were sampled through the upper 200 m of the water column for nutrient analysis every time a nitrogen fixation

experiment was carried out. Water samples were collected in 15 mL polypropylene tubes, which were thoroughly rinsed with the sample before filling directly from the Niskin bottles, frozen on board (−20 °C), and analyzed ashore by colorimetric methods (Hansen and Koroleff 1999) in a 4-channel (phosphate, silicate, nitrate + nitrite, nitrite) Lachat Instruments QuikChem 8500 Series 2 autoanalyzer (Subramaniam and Krahnmann 2021). The limits of detection of the instrument were 0.03 μM for phosphate, 1.25 μM for silicate and 0.05 μM for nitrite/nitrate.

In 2016, between 4 and 17 depths were sampled from the surface or the bottom of the mixed layer to the bottom of the profile at almost each CTD cast performed along the 23° W section. As in 2015, samples were taken in 15 mL polypropylene tubes, frozen on board and measured ashore by colorimetric methods in a Seal QuAAtro Continuous Segmented Flow Analyzer (phosphate, silicate, nitrate + nitrite, nitrite) (Tanhua 2021). The limits of detection of the instrument were 0.008 μM for phosphate, 0.045 μM for silicate and 0.007 μM for nitrite/nitrate.

The nitracline and phosphocline were calculated by linear interpolation in all stations where at least four depths were available in the upper 200 m. The depth of the nutriclines were used as a simple and feasible proxy for the supply of both nitrogen and phosphorus to the euphotic layer. The ratio nitrate to phosphate was also used for defining the stations where a habitat suitable for diazotrophs was possible.

## Modeled soluble iron deposition

We used an intermediate complexity iron model to simulate the daily deposition rates of soluble iron. A detailed description of the Earth system modeling set up used for estimating soluble iron deposition is given in Hamilton et al. (2019). Briefly, the model simulates the emission, transport, acidic and organic processing, and deposition of iron from multiple sources including dust, wildfires, industry, transport, and metal smelting. Transient simulations were performed using the Community Atmosphere Model v6 (CAM6) and the Land Model v5 (CLM5), within the Community Earth System Model v2 (CESM2). Model resolution is 1.25° × 0.9° × 56 (longitude by latitude by vertical layers). Simulations followed the modeling framework setup of

Hamilton et al. (2020), but additionally extended until the end of 2016 in order to cover the observational period in this study. To represent the meteorological conditions related to the deposition events observed, we nudged the model meteorology to the Modern-Era Retrospective analysis for Research and Applications (MERRA). Desert dust emissions were modeled by the Dust Entrainment And Deposition module (Zender et al. 2003), updated to include dust mineralogy (Scanza et al. 2015), brittle fragmentation theory on mineral size fractions (Kok 2011; Scanza et al. 2015), a physical vertical dust flux theory (Kok et al. 2014; Hamilton et al. 2019), and the enhancement of particle sphericity on dust mass extinction efficiency (Kok et al. 2017), and thus dust aerosol optical depth in the visible band. Anthropogenic iron emissions are taken from the Rathod et al. (2020) dataset with a repeating cyclic 2015 emission rate for both simulated years examined in this study. Fire aerosol emissions are from the Fire Inventory from NCAR version 1.5 (FINNv1.5) (Wiedinmyer et al. 2011) dataset and observationally defined iron:black carbon ratios used to estimate the iron content in fire smoke (Hamilton et al. 2019). For all other anthropogenic aerosol emissions, data sets were taken from the Coupled Model Intercomparison Project (CMIP) historical climate pathways for 2015 and from the Shared Socioeconomic Pathways (SSP) scenario SSP585 for 2016. Model comparison with iron observations shows the model can predict the main features of total and soluble iron in the study region (Hamilton et al. 2019). Furthermore, the model has been calibrated against North Atlantic iron isotope measurements to represent the fractional contributions of natural dust against anthropogenic iron aerosol sources (Conway et al. 2019). Detailed comparisons of simulated dust aerosol properties and burdens with observations can be found in Li et al. (2022).

Subsequently, at each station, total soluble iron daily deposition rates (wet+dry) were averaged over the 15 days previous to the sampling date, producing a rolling average along track. For both cruises, we used the model data within the grid boxes centered at 22.5° W for stations along the 23° W section. In 2016, the modeled data at the boxes at 21.25° W were used for the stations along the Guinea Dome core.

## Natural abundance of carbon and nitrogen stable isotopes in seston

For both cruises, the relative abundances of the stable isotopes of carbon ( $^{13}\text{C}/^{12}\text{C}$ ) and nitrogen ( $^{15}\text{N}/^{14}\text{N}$ ) were determined in seston samples collected by Niskin bottles at 1–5 depths in the upper 200 m of the water column. A variable volume of 1.8–14.2 L, depending on the density of material collected on the filter and availability of water, was gently filtered through pre-combusted (4 h, 450 °C) 47 mm GF/F filters (0.7 µm pore size). Filters were subsequently transferred to an oven at 60 °C until they were completely dried, and then stored in an airtight container until analysis. Prior to analysis, filters were trimmed for removing the particle-free edge and, based on the total biomass collected on the filtration area, a quarter, three quarters or the whole filter was pelletized into tin capsules.

The natural abundance of carbon and nitrogen stable isotopes was measured by continuous-flow isotope-ratio mass spectrometry (CF-IRMS) using a Micromass Optima interfaced to a Carlo Erba elemental analyzer (CE NC2500) in 2015, and a Micromass Isoprime IRMS coupled to a Carlo Erba elemental analyzer (NA 2500) in 2016. All carbon and nitrogen abundances were expressed in  $\delta$  notation (‰) relative to Vienna Pee Dee Belemnite (VPDB) and atmospheric  $\text{N}_2$ , respectively. The stability of the instrument and the contribution of any blanks to our measurements were checked using a series of elemental (methionine) and isotopic (peptone) standards placed every three samples in each analytical run (Montoya et al. 2008).

A two-end-member mass balance was used for estimating the carbon contributed by *Trichodesmium* to seston. The end members were the average signature of biomass produced by primary producers in the upper ocean,  $\delta^{13}\text{C}_{\text{pp}} = -22.0\text{‰}$  (Chanton and Lewis 2002; Chasar et al. 2005), and the average signature of *Trichodesmium* measured in the Sargasso and Caribbean seas,  $\delta^{13}\text{C}_{\text{trich}} = -12.9\text{‰}$  (Carpenter et al. 1997), applied to the following model.

$$\% \text{of } Trichodesmium\text{C} = 100 \times \frac{\delta^{13}\text{C}_s - \delta^{13}\text{C}_{\text{pp}}}{\delta^{13}\text{C}_{\text{trich}} - \delta^{13}\text{C}_{\text{pp}}}$$

where  $\delta^{13}\text{C}_s$  is the signature of the samples. All the samples included in this calculation were within the

range defined by these two end members. The  $\delta^{13}\text{C}_{\text{pp}}$  used is a good representative of seston containing a mixture of primary producers composed by phytoplankton with enriched values like diatoms ( $-17\text{‰}$ , Pancost et al. 1997) or more deplete values like *Synechococcus* ( $-24\text{‰}$  or less, Hansman and Sessions 2016), where the final signature of the community is a weighted mean of about  $-22\text{‰}$  in marine system, as stated above.

#### *Trichodesmium* colonies and potential contribution to nitrogen fixation

During both cruises, the abundance of *Trichodesmium* colonies larger than 500  $\mu\text{m}$  equivalent spherical diameter (ESD) in the water column was obtained by an Underwater Vision Profiler 5, UVP5, (Picheral et al. 2010) mounted on the rosette. Briefly, the UVP5 is an imaging profiler able to record images of particles larger than 500  $\mu\text{m}$  in diameter every 10 cm in the vertical when deployed at a speed of 1  $\text{m s}^{-1}$ . All image data were assigned to taxonomic categories (including *Trichodesmium* puffs and tufts colonies) using random forest algorithms and validated by experts on the web-based platform Ecotaxa (Picheral et al. 2017). *Trichodesmium* colony abundances ( $\text{colonies L}^{-1}$ ) were then binned in 5 m depth bins.

For qualitatively assessing the likelihood of these *Trichodesmium* colonies as the dominant nitrogen fixer in surface communities along the transects, we applied an indirect approach. We used the literature compilation of *Trichodesmium* specific rates in different locations of the Atlantic Ocean, done by Mulholland et al. (2006) in Table 7, for estimating colony-specific rates of nitrogen fixation by *Trichodesmium* colonies in  $\text{nmol N col}^{-1} \text{d}^{-1}$ . Once all the rates were transformed to the same units, we determined the 25th and 75th percentiles (1.4 and 6  $\text{nmol N col}^{-1} \text{d}^{-1}$ , respectively) of this dataset as conversion factors for a potential lower and upper limit of nitrogen fixation by *Trichodesmium*, respectively. We decided to develop this approach for representing the potential rates of natural populations containing individuals at different physiological states. Multiplying these conversion factors by the average abundances of colonies measured by the UVP5 in the three bins of the upper 15 m, we obtained a potential range estimate for the rate of nitrogen fixation that could be attributed to *Trichodesmium* colonies. It should be noted that this

is a qualitative measure for assessing if *Trichodesmium* colonies were the dominant contributors to the community nitrogen fixation measured along track. The principle underlying this approach is that, if the observed rates fall within the potential range attributed to *Trichodesmium* colonies and only if they do, it is very likely that they are the dominant diazotrophs.

#### Nitrogen fixation

The rates of size-fractionated nitrogen fixation of the planktonic community were determined following the  $^{15}\text{N}_2$  technique as proposed by Montoya et al. (1996) at 29 stations in 2015 and 43 stations in 2016 (Fig. 1). At each station, triplicate 4.4-L acid-washed clear polycarbonate bottles (Nalgene) were filled directly from the Niskin bottles with water from 1 to 4 depths. After carefully removing all air bubbles, 3 ml of  $^{15}\text{N}_2$  (98 atom%, Cambridge Isotopes Lot. #I-19168A), whose pressure was equilibrated to atmospheric, were directly injected to each bottle as a bubble of gas. The bottles were incubated 24-h on-deck in a system of re-circulating water from the ship's clean supply, and simulating in situ PAR levels (60, 30, 20, 10, 1 or 0.1% depending on the depth) by a combination of blue and neutral density screens in 2015 and neutral density meshes in 2016. After, 24 h the whole volume of the bottle was sequentially filtered through a 10  $\mu\text{m}$  acid-washed nylon mesh and a pre-combusted (4 h, 450  $^\circ\text{C}$ ) 25 mm GF/F filter (0.7  $\mu\text{m}$  pore size). The particles collected in the 10  $\mu\text{m}$  nylon mesh were then washed with GF/F filtered sea water onto a pre-combusted (4 h, 450  $^\circ\text{C}$ ) GF/C filter (1.2  $\mu\text{m}$  pore size) and filtered under low vacuum pressure ( $<50 \text{ mm Hg}$ ). Both filters were completely dried at 60  $^\circ\text{C}$ , and stored in an airtight container. Whole filters were pelletized, after trimming the particle-free edge, for assuring that all the particles incubated were analyzed. The analyses of particulate nitrogen content and  $^{15}\text{N}$  atom% were carried out in the same instruments and following the same procedure mentioned in the natural abundance stable isotopes section.

The initial concentration of  $\text{N}_2$  dissolved in seawater was estimated using the equations of Weiss (1970) and assuming equilibrium with the atmosphere. The equations proposed by Montoya et al. (1996) were used for calculating the rates of nitrogen fixation, and the detection limit of the technique (0.05  $\text{nmol N L}^{-1} \text{d}^{-1}$  in both cruises). Seston samples

for the determination of stable isotopes of nitrogen taken at the same depths as the nitrogen fixation rate experiments were used as time zero for these calculations. A single detection limit was estimated for each cruise using the combination of variables that defined the highest possible threshold in our experiments, that is, we used an acceptable change of 4‰ in the particulate nitrogen over the course of incubation time, the lowest enrichment in  $^{15}\text{N}$  of the dissolved nitrogen gas pool ( $\text{AN}_2\%$ ), the shortest incubation time, and the highest particulate nitrogen found at the end of incubation.

Previous studies suggest that the traditional bubble addition technique underestimates the rates due to a low dissolution of the bubble, meaning that the  $^{15}\text{N}_2$  available to nitrogen fixers during the incubation is lower than calculated (Mohr et al. 2010; Grosskopf et al. 2012; White et al. 2020). However, the degree to which this partial dissolution of the bubble leads to an underestimation of the rates remains inconclusive. This depends on several factors, including temperature, salinity, volume of injected  $^{15}\text{N}_2$  and volume incubated, and still need to be addressed by further studies comparing both methods (Shao et al. 2023). In this sense, the disparity of methodologies and limited number of dissolution curves available in the literature makes the calculation of the underestimation a challenging task (Mohr et al. 2010; Jayakumar et al. 2012; Wannicke et al. 2018). Therefore, the rates shown in this study should be considered as a conservative, but valuable, lower end estimate of diazotrophy in the Guinea Dome and Equatorial Atlantic Ocean.

#### Databases, statistics and graphs

The version 2 of the global oceanographic database of diazotrophs was used for comparison with our data in a region between  $15^\circ\text{N}$ – $5^\circ\text{S}$  and  $15^\circ$ – $25^\circ\text{W}$  (Shao et al. 2023). We also included the rates presented in Voss et al. (2004), measured in our region of study. Hence, most of the rates available in the box defined above were discussed in six publications (Voss et al. 2004; Grosskopf et al. 2012; Subramaniam et al. 2013; Martínez-Pérez et al. 2016; Fonseca-Batista et al. 2017; Singh et al. 2017). Additionally, Shao et al. (2023) also contains nine stations measured during the Atlantic Meridional Transect in May–June 2004 by Dr. A.P. Rees, that are

unpublished. Therefore, in this region of the eastern tropical Atlantic Ocean, there are only seven surveys, which provide rates retrieved from May to November, i.e., late spring to late fall, between 2002 and 2013.

Non-parametric statistical correlation by Spearman Rho, parametric t-test, non-parametric Wilcoxon test and plots were made using R Studio and the ggplot2, ggpubr and oce packages (Kelley 2011; Gómez-Rubio 2017; Kassambara 2018; Rstudio 2020). The parametric or non-parametric tests were chosen after testing our datasets for normality.

## Results

### Hydrography, zonal currents and nutrients

The meridional distribution of hydrographic properties along  $23^\circ\text{W}$  was similar during both cruises (Fig. 2). In the northern end of the transect in the Guinea Dome region ( $9^\circ$ – $15^\circ\text{N}$ ), isotherms shoaled, and the mixed layer was shallower. Isotherms deepened gradually from ca.  $9^\circ\text{N}$  to about  $2^\circ\text{N}$ , and then shoaled slightly at the southern end of the transect toward  $5^\circ\text{S}$ . The thermocline, i.e., the region of maximum vertical temperature gradient, was located close to the mixed layer depth at most stations except for a few stations around the Equator. In the band  $4^\circ$ – $9^\circ\text{N}$ , warmer and fresher waters ( $>26^\circ\text{C}$ , around 35.2 PSU) marked the North Equatorial Countercurrent, which was evident as an eastward current band in the zonal velocities measured by the ADCP (Fig. 2). A maximum of salinity ( $>36$  PSU) around  $0^\circ\text{N}$  at ca. 100 m depth marked the core of the Equatorial Undercurrent for both cruises, present as a strong eastward current in the zonal velocities (Fig. 2). There were differences in salinity between the two cruises with the freshest water of the North Equatorial Countercurrent found at  $7^\circ$ – $8^\circ\text{N}$  in September 2015 and at  $4^\circ$ – $5^\circ\text{N}$  in August–October 2016. The maximum of CTD fluorescence was used as a proxy for the deep chlorophyll maximum (DCM). During both cruises, this DCM was more intense and shallower in the Guinea Dome region (Fig. 2), deepening southward between  $9^\circ$  and  $2^\circ\text{N}$ . In the region between  $2^\circ\text{N}$  and  $6^\circ\text{S}$ , there were instead substantial differences in the depth and intensity of the DCM when comparing the 2015 and 2016 cruises.

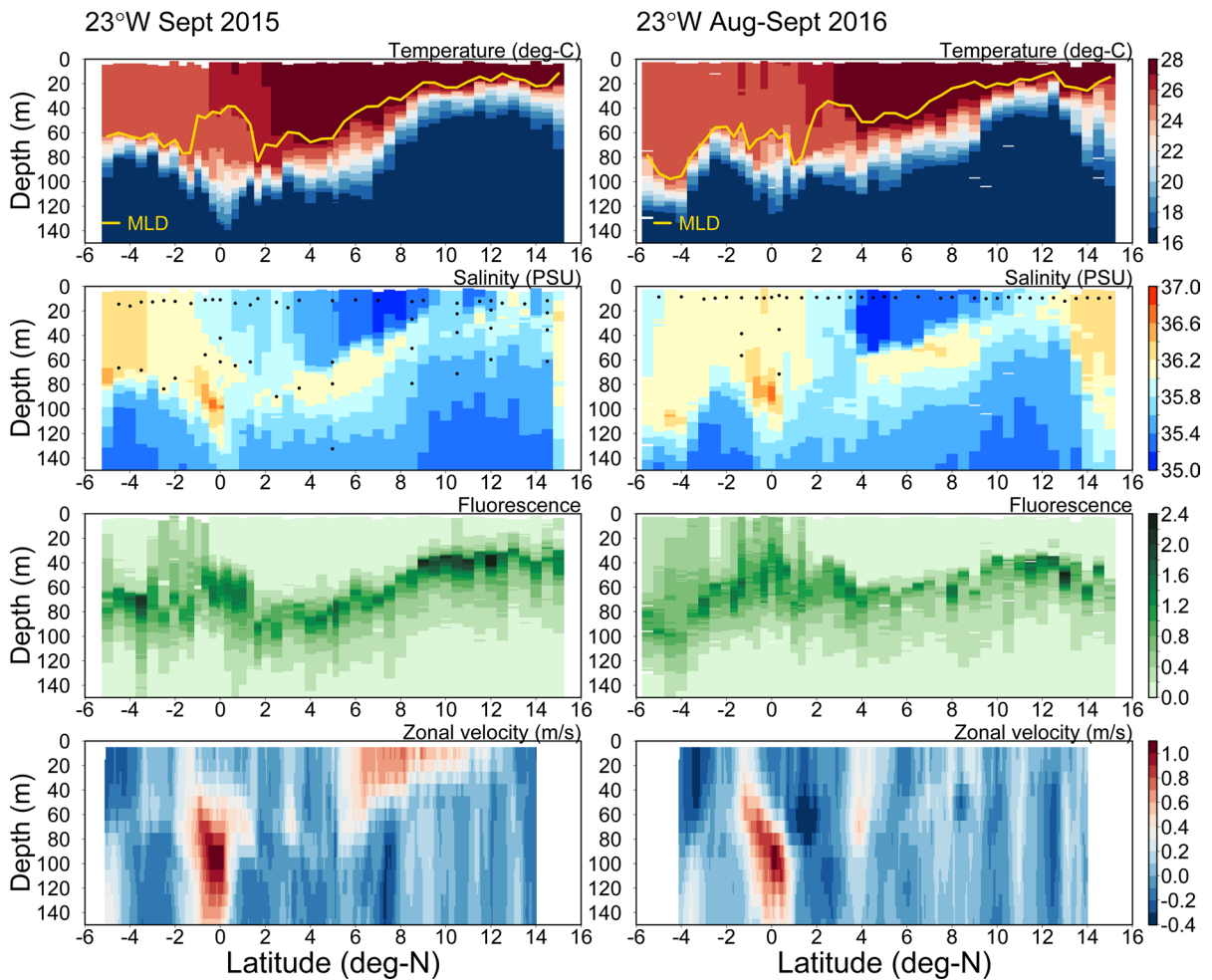


**Fig. 2** CTD temperature, salinity, chlorophyll *a* fluorescence, and vessel mounted acoustic Doppler current profiler (75 kHz) zonal currents sections along 23° W in September 2015 (left) and August–September 2016 (right) cruises. The yellow solid line in the temperature panel represents the depth of the mixed

layer estimated by the approximation of Kara et al. (2000). The black dots in the salinity panel represent the depths sampled for nitrogen fixation rate experiments. Positive values in the zonal velocity plots represent eastward currents, and negative values represent westward currents

The hydrographic structure at the Guinea Dome deep mooring site (11° N) was slightly different between the two cruises with the base of the mixed layer and the DCM being slightly shallower in 2015 than in 2016 (Fig S1), similar to what is seen along the 23° W section. In 2016, additional stations were sampled around the core of the Guinea Dome, where the mixed layer was shallow (<40 m) and warm (>26 °C), salinity ranged between 35 and 35.5 PSU, and the DCM was relatively shallow (Fig S1).

For both cruises, meridional distributions of nitrate and phosphate along 23° W showed similar patterns (Fig. 3). At most stations, surface samples

were below detection limit for nitrate, but contained measurable phosphate, meaning a very low nitrogen to phosphate ratio (N:P) near the surface. Using the detection limits mentioned in the methods section as the threshold for this ratio, N:P near the surface was an unknown value below 1.7 in 2015 and 0.9 in 2016. This nutrient depleted upper layer was shallower at the northern end of the transect, deepened gradually towards the Equator, and shoaled again further to the south (Fig. 3). Larger differences between the nitra-cline and the phosphocline were observed between 4° N and 4° S (Fig. S2). At the southern end of the transect (south of 6° N), we tested the significance



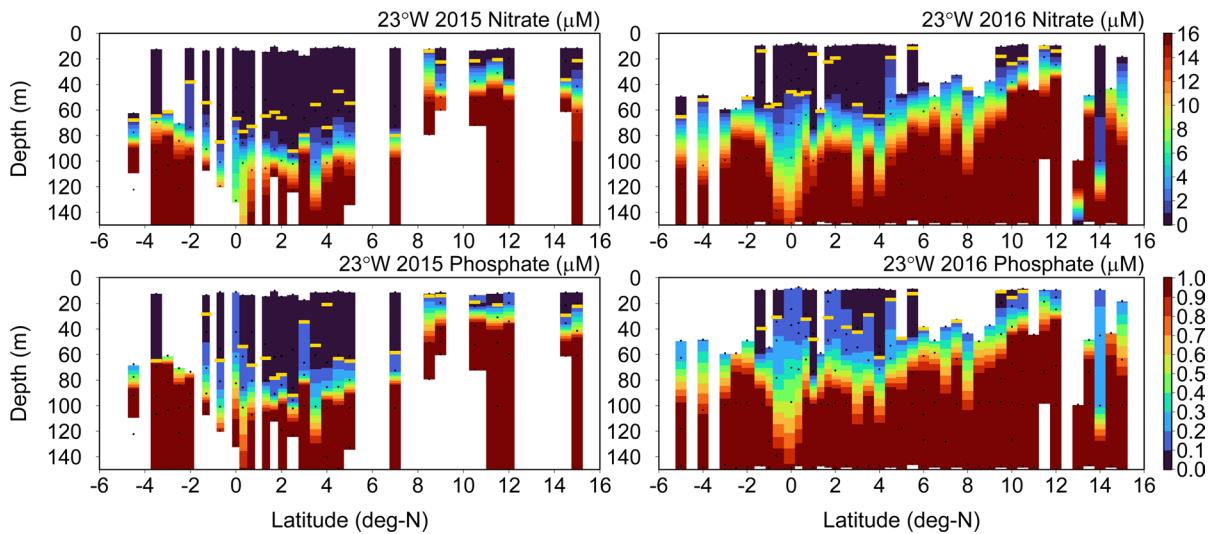


**Fig. 3** Vertical distribution of the concentrations of nitrate ( $\mu\text{M}$ ) and phosphate ( $\mu\text{M}$ ) measured along  $23^\circ\text{W}$  in 2015 (left) and 2016 (right) cruises. Yellow dash represents the depth of the nitracline or phosphocline calculated by linear interpola-

tion using  $1\ \mu\text{M}$  (nitrate) and  $0.1\ \mu\text{M}$  (phosphate) as the thresholds. Note that in some stations in the phosphate panels the actual concentration at the first depth was above this threshold of  $0.1\ \mu\text{M}$ , and therefore there is no dash

of the observed difference in the depth of each nutri-  
cline between years by a two-sample t-test. The t-  
tests showed that the 2015 nitracline (mean=65.7,  
standard deviation=13.5,  $n=19$ ) and phosphocline  
(mean=59.0, standard deviation=19.7,  $n=19$ )  
were significantly deeper than the 2016 nitracline  
(mean=42.7, standard deviation=19.7,  $n=25$ ) and  
phosphocline (mean=36.2, standard deviation=13.2,  
 $n=25$ ), respectively. The t-statistic for the compar-  
ison of nitraclines was 4.1 with  $df=34$  ( $p<0.01$ ).  
The t-statistic for the comparison of phosphoclines  
was 3.5 with  $df=25$  ( $p<0.01$ ). At the stations  
across the core of the Guinea Dome in 2016, the  
distributions were similar to those at  $23^\circ\text{W}$ , with  
a shallow nutrient depleted upper layer at the north-  
ern end (ca.  $12^\circ\text{N}$ ) that deepened slightly toward  
the southern end at ca.  $8^\circ\text{N}$  (data not shown). It  
should be noted that the dataset of nutrients taken  
along the cruise track in 2015 had more gaps than  
in 2016 due to the failure of instruments and loss  
of samples during transport to the laboratory.

The modelled 15-day rolling average of soluble  
iron deposition from the atmosphere showed a  
similar trend along both the 2015 and 2016  
cruise tracks. Higher deposition rates (a tenfold  
in 2015, and a 20-fold in 2016, on average) were  
predicted in the region of the Guinea Dome ( $14^\circ$ – $7^\circ\text{N}$ )  
closer to

North African dust sources compared to south of  
 $4^\circ\text{N}$  (Fig. 4) which are further away. However,  
there were interannual differences between years  
in the strength of this flux. In 2015 the flux was  
a 1.4-fold lower than in 2016 between  $13^\circ$  and  
 $4^\circ\text{N}$ , but by contrast, higher by a 1.4-fold  
between  $2^\circ\text{N}$  and  $2^\circ\text{S}$ . It should also be noted  
that while the soluble iron deposition rates would  
be expected to be higher closer to the African  
coast at the core of the Guinea Dome at around  
 $21^\circ\text{W}$ , instead the model predicts higher deposi-  
tion rates a little further west along  $23^\circ\text{W}$  (Fig. 4).

#### *Trichodesmium* abundance and contribution to phytoplankton carbon

The highest abundances of *Trichodesmium* colonies  
were found in the area of the Guinea Dome  
between  $9^\circ$  and  $15^\circ\text{N}$  (Fig. 4). The maximum  
abundance of colonies was near the surface in  
all but two stations: in 2015 at  $3^\circ\text{N}$   $23^\circ\text{W}$ , and  
in 2016 at  $9^\circ\text{N}$   $23^\circ\text{W}$ , where it was at ca. 50  
and 30 m, respectively (Fig. 4). Abundances  
were similarly high near the surface in the core  
of the Guinea Dome.

In both cruises, the contribution of *Trichodes-*  
*mium* carbon to the  $\delta^{13}\text{C}$  of seston in surface  
ranged between 15 and 25% in the Guinea Dome  
region along the  $23^\circ\text{W}$  section (Fig. 4), suggest-  
ing that

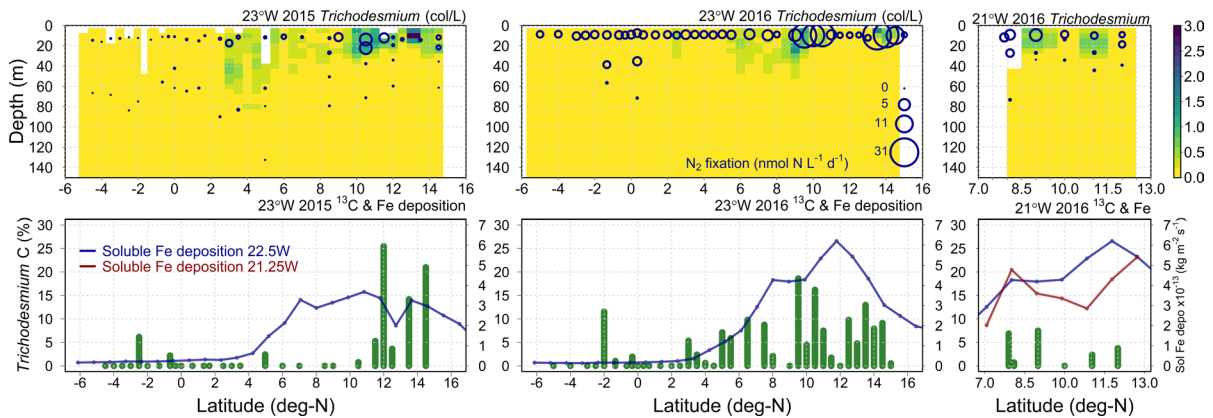


**Fig. 4** *Trichodesmium* concentration, nitrogen fixation rates, percent contribution of *Trichodesmium* to seston carbon and soluble Fe deposition along 23° W and approximately 21° W (Guinea Dome core). **Upper panels:** the colored background bars represent the abundance of *Trichodesmium* colonies (puff + tuft morphologies) identified by the Underwater Vision Profiler 5 (colonies  $L^{-1}$ ), and the bubbles represent the rates of measured total nitrogen fixation ( $nmol\ N\ L^{-1}\ d^{-1}$ ). **Lower panels:** contribution of *Trichodesmium* carbon to the signatures of  $\delta^{13}C$  of seston estimated by a two-end-member mass bal-

ance based on *Trichodesmium* ( $-12.9\ ‰$ ) and organic matter produced by primary producers in the upper ocean ( $-22\ ‰$ ) as end-members. The solid lines in these panels represent the 15-day rolling average of modeled total soluble iron deposition ( $\times 10^{-13}$  in  $kg\ m^{-2}\ s^{-1}$ ) estimated along 22.5° W in 2015 and 2016, and along 21.25° W for the Guinea Dome section in 2016. Note that, in the Guinea Dome section panel on the bottom right, both fluxes are represented for comparison, in blue the deposition at 22.5° W and in red the deposition at 21.25° W

*Trichodesmium* was an important component of the phytoplankton community here. In addition, this stable isotope approach points to a contribution of *Trichodesmium* at some stations south of 6° N, especially around 2° S. Here the UVP5 did not record colonies larger than 500  $\mu m$ , but the community could be composed mostly of free trichomes, not detectable by the UVP5. The contribution of *Trichodesmium* was greater in 2016 at most stations north of 5° N compared to 2015.

In 2016, the distribution of *Trichodesmium* colonies in the transect done at the core of the Guinea Dome was similar to that observed along 23° W, with a maximum of colonies in the upper 20 m at 9° N. However, the contribution of *Trichodesmium* to seston carbon at the surface here was lower, ranging from 1 to 5% (Fig. 4).

#### Nitrogen fixation

In 2015, the sampling scheme was designed for reaching a balance between the highest spatial resolution, horizontally along track (29 stations in latitudinal section) and by depth vertically (15 stations with depth profiles), given the logistical constraints of water budgets and sampling (Fig. 4). In 2016, emphasis

was placed on a finer horizontal along track resolution for resolving the meridional pattern on this finer spatial scale (43 stations, Fig. 4), but with fewer stations sampled at multiple depths (two stations along 23° W, and six along the section at the Guinea Dome core, Fig. 4). Using the stations where measurements were made at multiple depths (i.e., at least three), we found a statistically significant correlation between the vertically integrated nitrogen fixation and surface nitrogen fixation rates (Spearman Rho 0.89,  $p < 0.01$ ,  $n = 13$ ).

Nitrogen fixation rates ranged from below detection limit (i.e.,  $< 0.05\ nmol\ N\ L^{-1}\ d^{-1}$ , which was represented as 0) to almost  $31\ nmol\ N\ L^{-1}\ d^{-1}$ . The lowest rates were found at depth (0.1% PAR depth) and also at stations south of 3° N in 2015. The highest rates were found near the surface in the Guinea Dome region along 23° W. In general, higher rates were found in stations with higher abundances of *Trichodesmium* colonies (Fig. 4).

A closer look at the rates measured at the surface shows the differences and similarities between 2015 and 2016. In both cruises, the highest rates along 23° W were found in the region of the Guinea Dome, with a decrease towards the Equator. But while in 2015 the rates were very low, often

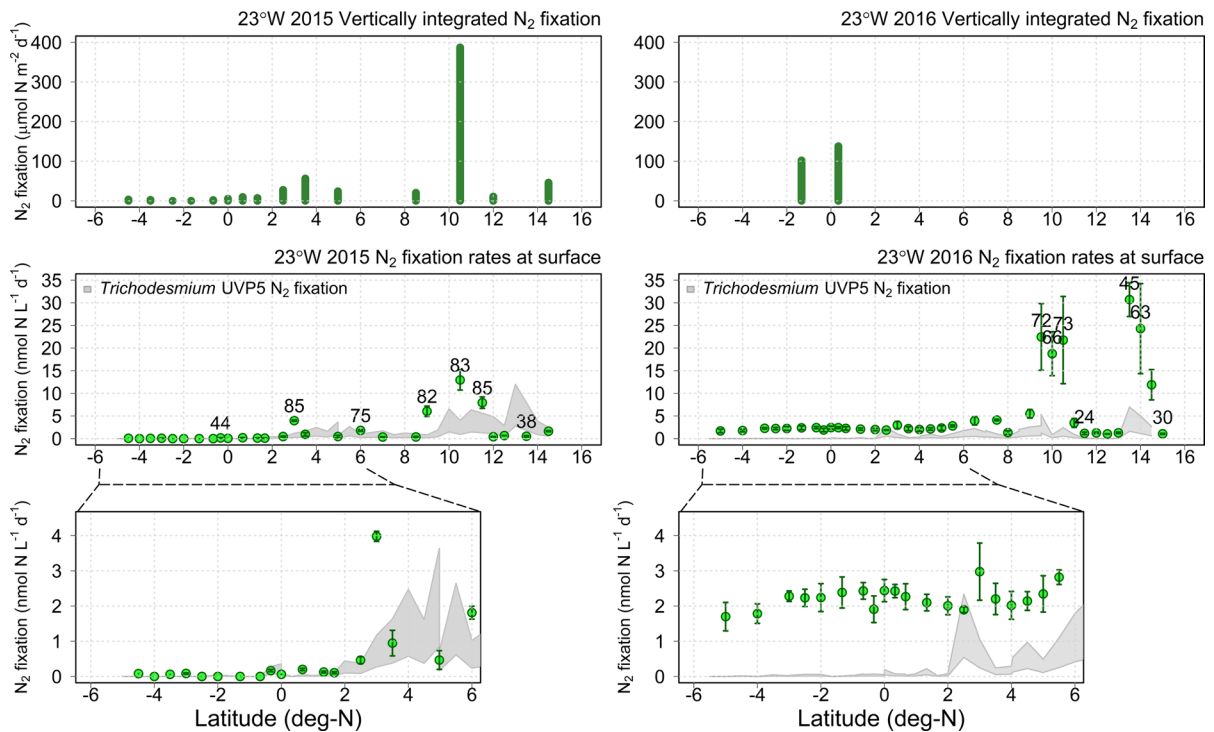


**Fig. 5** Nitrogen fixation rates along 23° W in 2015 (left panels) and 2016 (right panels). In the *upper panels*, the bars represent the vertically integrated total nitrogen fixation down to the deep chlorophyll maximum in those stations where at least two depths were sampled throughout the water column, as shown in Fig. 4. In the *middle panels*, green circles represent the rates of in situ measured total community nitrogen fixation at surface (ca. 10 m); the shadowed areas represent

the estimated rates of nitrogen fixation due to the average of *Trichodesmium* colonies identified by the Underwater Vision Profiler 5 (UVP5) in the upper 15 m; the black numbers represent the % contribution of the > 10  $\mu\text{m}$  size fraction to total community nitrogen fixation in the stations where it was above 10%. The *lower panels* present a zoom of the middle panels in the band 6° N–6° S for better showing the distribution of the low rates (< 5  $\text{nmol N L}^{-1} \text{d}^{-1}$ ) found in this region

below the detection limit, with no apparent pattern between 6° N and 5° S, the rates in 2016 showed a wave-like pattern and were twofold higher (Fig. 5). At the stations near the core of the Guinea Dome at approximately 21° W in 2016, rates were lower than those measured at the same latitudes along 23° W, but higher than the ones found at the Equatorial band (Fig. 4). At most of the stations along 23° W, the < 10  $\mu\text{m}$  size fraction was the main contributor to the nitrogen fixation rates at the surface (Fig. 5), with the exception of the area near the Guinea Dome and a few stations between 6° N and 5° S in 2015, where the contribution of the large size fraction to nitrogen fixation ranged between 24 and 85%. It is to be noted that these rates were above the range estimated for *Trichodesmium* colonies (shaded area in Fig. 5). Vertically integrated

rates down to the deep chlorophyll maximum are moderate except at the 11° N station in 2015, where the highest rates of that cruise were measured at the surface and mixed layer depth samples (Fig. 4) reaching almost 390  $\mu\text{mol N m}^{-2} \text{d}^{-1}$  (Fig. 5).

The distribution of potential nitrogen fixation rates related to *Trichodesmium* colonies pictured by the UVP5 showed a distribution similar to that of the in situ measured total community rates (Fig. 5, gray area). Higher rates with larger variability in this qualitative description were predicted for the colonies in the Guinea Dome region. However, in situ rates were consistently higher than those attributed to *Trichodesmium* colonies (Fig. 5, green circles). The UVP5 detected few colonies south of 2° N in 2015 and 2016, resulting in almost negligible rates for *Trichodesmium* in this region (Fig. 5).

## Discussion

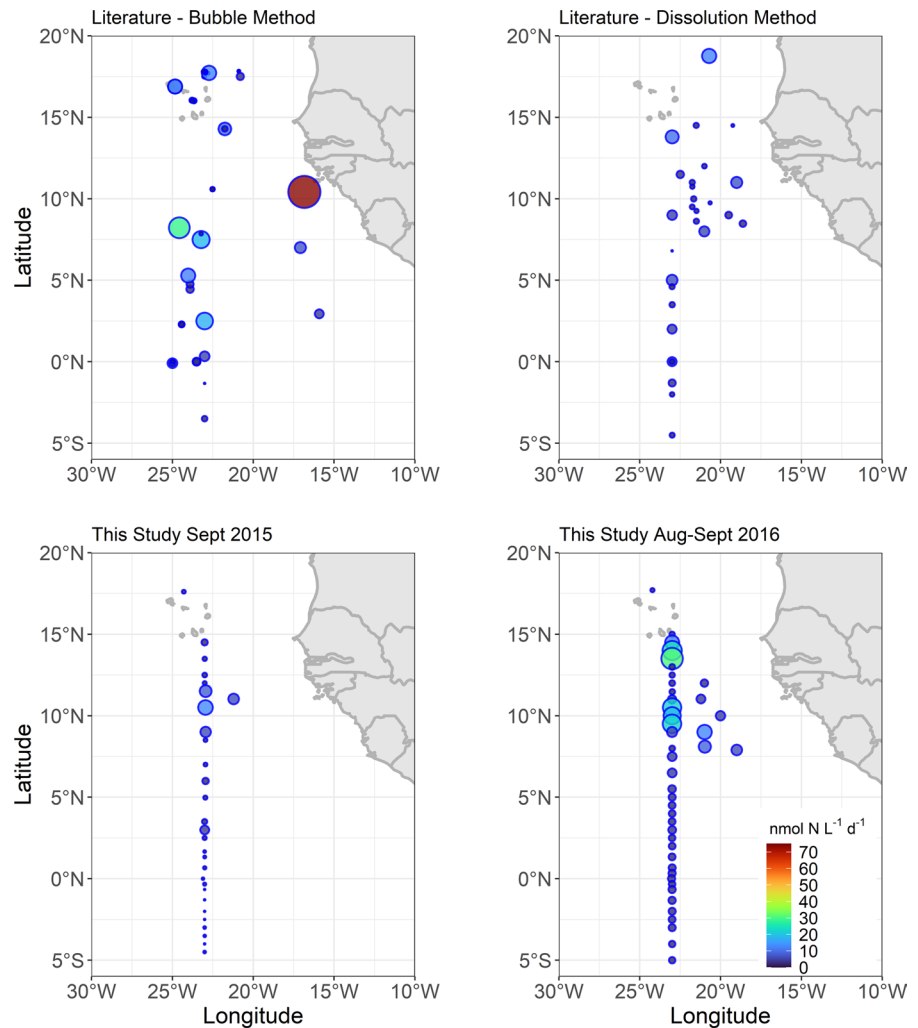
The central tropical Atlantic Ocean is a dynamic region with several strong zonal currents flowing in opposite directions, whose strengths vary seasonally (Fig. 1, e.g., North Equatorial Current, North Equatorial Countercurrent, northern branch of the South Equatorial Current, Equatorial Undercurrent, and the central branch of the South Equatorial Current). These currents are prone to flow instability forming tropical instability waves in the equatorial region and around 5° N (von Schuckmann et al. 2008). Additionally, eddies are shed from the eastern boundary particularly affecting the water mass properties in the region of the Guinea Dome (Schütte et al. 2016). The most prominent atmospheric feature is the northward movement of the Inter Tropical Convergence Zone (ITCZ) which controls the delivery of iron in the form of wet and dry deposition. The ITCZ moves from about the Equator to around 12° N in late boreal spring/early summer and then return to the Equator in late boreal fall (Mitchell and Wallace 1992). The occurrence of near-inertial waves forced by resonant wind forcing is also interesting to note. These interactions drive short-lived upper ocean mixing events between June–September, that are able to enhance the nutrient fluxes to the upper ocean by a factor of 20–50 for a few days (Hummels et al. 2020). The different physical processes have an important impact on the biogeochemistry of the central tropical Atlantic, both through large scale features such as the Equatorial Cold Tongue, but also at smaller spatial and temporal scales than previously described.

A high spatial resolution sampling is essential for bridging the current gap between small scale processes and global estimates (Benavides and Robidart 2020). For our study, its importance can be seen in both the changes in physical and chemical variables along the section as well as in the difference between 2015 and 2016 (Figs. 2, 3). For example, the changes between years in the strength and positioning of the North Equatorial Countercurrent and the northern branch of the South Equatorial Current are evident in the salinity and zonal velocity distributions (Fig. 2). However, they may not be obvious in a coarser resolution sampling scheme—either spatial such as the Atlantic Meridional Transect cruises (Rees et al. 2015), or temporal such as the GoShip cruises (Sloyan et al. 2019), both typical of annual basin scale

sections. The relationship between subtle changes in surface ocean circulation and consequent changes in nutriclines may also be missed in coarse samplings. While the nutrient data from 2015 presents several gaps due to the failure of instruments and loss of samples, both nitracline and phosphocline were significantly shallower in 2016 compared to 2015 with consequences for biogeochemistry and nitrogen fixation (Fig. 3, Fig. S2). Our increased resolution, especially in 2016, should have been sufficient to catch the effect of sub- and mesoscale structures, for instance anticyclonic eddies, known to enhance diazotrophy (Fong et al. 2008; Loescher et al. 2016). However, we only observed an anticyclonic mode water eddy crossing the 23° W section at 8° N in 2015 (Christiansen et al. 2018), in the part of the section with the coarser resolution, while none was affecting us directly at the time of sampling in 2016 (Fig. S3). Still, the importance of our high spatial resolution sampling is especially obvious in the range of variability in measured nitrogen fixation rates in the Guinea Dome and equatorial upwelling regions. We provide a total of 72 stations in our region of study between 20° N–5° S 15°–25° W, four more than those compiled by Shao et al. (2023) complemented with Voss et al. (2004) as it can be seen in Fig. 6. This resolution was able to resolve the patchiness of the Guinea Dome in 2016, a variability in plankton metabolism that is not obvious or does not always appear when the stations are separated every 3 or 4 degrees of latitude/longitude (e.g., Fig. 2a in Moore et al. 2009, Fig. 7c in Fernández et al. 2010, or Fig. 10 in Marañón et al. 2000), but emerges in high resolution schemes like ours or, for instance, Shiozaki et al. (2014). A simple way for illustrating how easily variability like that at the Guinea Dome is lost in coarser schemes could be done by comparing our rates at surface with those measured by Grosskopf et al. (2012). This study was done during Meteor cruise M80-81 along 23° W in boreal fall 2009 using the dissolution method (Fig. S4).

*Trichodesmium* has been extensively studied during the last 30–40 years, and therefore, its environmental and nutrient requirements for growth and active nitrogen fixation are well-defined. In particular, *Trichodesmium* thrives in shallow mixed layers with temperatures above 20 °C with sufficient supply of iron and phosphorus (Capone et al. 1997; Berman-Frank et al. 2001; Kustka et al. 2003; Tyrrell

**Fig. 6** Total community nitrogen fixation measured at surface (< 15 m) in previously published studies (Voss et al. 2004; Grosskopf et al. 2012; Shao et al. 2023; Luo et al. 2012; Subramaniam et al. 2013; Martínez-Pérez et al. 2016; Fonseca-Batista et al. 2017; Singh et al. 2017) explained in the methods section (upper left studies using the bubble method, upper right studies using the dissolution method), and in 2015 (bottom left) and 2016 (bottom right) cruises. The units of previously published rates were converted to  $\text{nmol N L}^{-1} \text{d}^{-1}$ , whenever necessary



et al. 2003; Mills et al. 2004; Mulholland and Bernhardt 2005; Breitbarth et al. 2007; Stal 2009). It has developed unique strategies for keeping its buoyancy, adapting to high light and accessing iron directly from dust particles (Held et al. 2022). Therefore, the distribution of colonies during our cruises in 2015 and 2016 is not entirely surprising (Fig. 4). Here, the maxima of abundance were found in the Guinea Dome area, associated with shallower and warmer mixed layers with a higher supply of iron from dust deposition as well as still sufficient phosphorus (Figs. 3, 4). Due to their gas vesicles, *Trichodesmium* colonies tend to concentrate in surface waters during the late stages of blooms, similar to what we found at 13° N 23° W. However, subsurface maxima, like those at 50 m at 3° N in 2015 and at 30 m at 9° N

in 2016 (Fig. 4), were previously described in the literature when the organisms are still able to control their buoyancy (Villareal and Carpenter 1990; Carpenter and Capone 1992). In November 2009, Grosskopf et al. (2012) also found high *nifH* expression of *Trichodesmium* in the Guinea Dome area with a maximum in the surface layer at 9° N 23° W. In addition, Sandel et al. (2015), using the same UVP5 along 23° W in November 2012, found the highest abundance of *Trichodesmium* colonies ( $> 2 \text{ col L}^{-1}$ ) between 3° and 9° N. Hence, both studies support the fact that this genus is present at varying abundances here throughout the year. Nevertheless, it is important to note that the UVP5 only detects large colonies ( $> 500 \mu\text{m}$ ), which in some regions can represent a small fraction of the population, that is mostly

comprised of free trichomes and/or smaller colonies (Carpenter et al. 2004; Fernández et al. 2010). The absence of *Trichodesmium* colonies near the Equator (2° N–6° S) as well as an almost negligible contribution of the > 10 µm size fraction to the rates of nitrogen fixation point to a change in the composition of the diazotroph community probably to small diazotrophs. However, we cannot disregard completely the presence of *Trichodesmium* in this southern end of the transect, where the UVP5 barely detected colonies. In 2016 at 0.36° S, 44% of the nitrogen fixation was supplied by the > 10 µm size fraction. This points to the presence of free *Trichodesmium* filaments (Fig. 5). In general, the carbon isotopes ( $\delta^{13}\text{C}$ ) confirm the distribution of *Trichodesmium* mentioned above. This genus contributed more carbon to particles in the Guinea Dome region (up to 25%), but there was almost no imprint in the equatorial band between 5° N and 5° S (Fig. 4), again suggesting that this genus frequently flourishes in the dome.

In the different locations where nitrogen fixation was assessed throughout the water column down to the deep chlorophyll maximum, the highest rate was consistently found in surface waters, except at a few stations in the Guinea Dome. Here, the rates in the upper 40 m were substantial and in the depths with higher abundances of *Trichodesmium* colonies and a predominant contribution of the > 10 µm size fraction to nitrogen fixation at surface (up to 85%, Fig. 5). In spite of that, the significant positive correlation between the vertically integrated and surface rates (Spearman Rho 0.89,  $p < 0.01$ ,  $n = 13$ ) points to a dominance of surface communities in the water column nitrogen fixation throughout the transect. This also suggests that the general pattern found in surface waters could be extrapolated to the euphotic layer throughout the whole transect. In this regard, the highest nitrogen fixation rates at the boundaries of the Guinea Dome around 13° and 10° N (Fig. 4, 5) were found in association with higher iron deposition rates (Fig. 4), low N:P (< 1.7) waters, and a phosphocline generally shallower than the nitracline (Fig. S2). This points to strong nitrogen limitation in the presence of sufficient iron and phosphorus to fulfill nitrogen fixers' requirements for active diazotrophy. The increased spatial resolution in surface waters in 2016 relative to 2015 revealed an interesting variability in the Guinea Dome region. While the pattern in 2015 suggests a maximum only at around

10° N, we found high rates at the northern end of the transect around 13° N 2016 (Fig. 5). However, the partitioning between the two size classes of diazotrophs is slightly different at the two locations. On the one hand, at about 10° N in both cruises, large diazotrophs (> 10 µm) are the major contributors to diazotrophy (ca. 70–80%). In this region, the rates attributable to *Trichodesmium* colonies are lower than the in situ rates, but the  $\delta^{13}\text{C}$  of particles reflects the presence of *Trichodesmium* even where the UVP5 could not see large colonies (> 500 µm). Therefore, it is possible that the population was mostly composed of free trichomes, smaller colonies or a combination of the two. On the other hand, at 13° N in 2016, the large size class contributed slightly less (ca. 40–60%) to total nitrogen fixation, and the absolute values were again higher than the qualitative rates of *Trichodesmium* colonies, suggesting the additional presence of other smaller active diazotroph groups during this survey. All this is consistent with previous studies of the *nifH* gene, showing that *Trichodesmium*, unicellular cyanobacteria (mainly group A) and gamma proteobacteria coexist and alternate their dominance in the region around 10° N (Langlois et al. 2005; Goebel et al. 2010; Rijkenberg et al. 2011; Grosskopf et al. 2012; Martínez-Pérez et al. 2016). In 2016, the distribution of nitrogen fixation in surface waters in the whole Guinea Dome region (Fig. 6) also shows higher rates at the southern end of the dome around 8°–9° N. Interestingly, it seems that the physicochemical processes at the boundaries of this atypical upwelling system enhance nitrogen fixation, likely supported by *Trichodesmium*. Still, further research is required for disentangling the drivers of this substantial and highly variable nitrogen fixation activity in the Guinea Dome.

In the southern half of the transect towards the Equator, nutrients along the cruise track depicted a setting similar to that of the Guinea Dome. In both cruises, the phosphocline was shallower than the nitracline (Fig. S2). This difference was also observed in an earlier transect cruise in the region (Sandel et al. 2015). At most stations, phosphate in the upper mixed layer was always measurable and above the threshold set for the phosphocline (0.1 µM), while nitrate was below detection limit (Fig. 3). Even though the lower resolution of nutrient measurements in 2015 complicates the comparison, the significantly shallower phosphocline in 2016 than in 2015 between

6° N and 5° S points to a higher supply of phosphorus to the surface in the second cruise (Fig. S2). By contrast, the 15-day rolling average of total soluble iron deposition was slightly lower in 2016 (Fig. 5). However, this difference is based on subtle changes in the daily deposition rates in the days prior to station (Fig. S5), and therefore, soluble iron deposition was virtually the same in both years between 6° N and 5° S. Although, wet deposition from rainfall associated to the Inter Tropical Convergence Zone has been shown to be a major source of dissolved iron to the tropical Atlantic (Schlosser et al. 2014), clear differences in precipitation between 2015 and 2016 only happened in the days before the stations between 3° and 5° N (Fig. S5). In addition, the patterns of precipitation and soluble iron deposition were similar, hence our modeled deposition rates seemed to capture the effect of the Inter Tropical Convergence Zone relatively well. Taking all this into account, the supply of phosphorus rather than that of iron would partially explain the almost twofold higher rates measured at surface in 2016 between 6° N and 5° S.

As we mentioned above, in spite of more than 50 years of research in diazotrophy in the Atlantic Ocean (Benavides and Voss 2015) and almost 60 years in the global ocean, the data available in the eastern central tropical Atlantic is still sparse (upper panels of Fig. 6). Here we represent all the rates at the surface ( $\leq 15$  m) from the limited number of studies available in the literature (Voss et al. 2004; Grosskopf et al. 2012; Subramaniam et al. 2013; Martínez-Pérez et al. 2016; Fonseca-Batista et al. 2017; Singh et al. 2017; Shao et al. 2023). It is to note that these measurements were done using different methodologies (e.g.,  $^{15}\text{N}_2$  bubble or dissolution methods), in different times of the year from May to November, and expressed in different units. Therefore, all rates were converted to  $\text{nmol N L}^{-1} \text{d}^{-1}$  for comparison with our data. In general, literature data suggest that the Guinea Dome is an area of low to moderate nitrogen fixation activity, with increased rates at the potential edges of the dome (around 15° N and 8° N). Most of our rates near the surface in the vicinity of the Guinea Dome (8°–15° N) during 2015 and 2016 fall within the upper bound of previous measurements (Fig. 6). A comprehensive look at the range of variability in this latitudinal band shows that there are very few studies in the literature providing rates higher than ours. It is worth noting that, Voss et al. (2004) and

A.P. Rees in Shao et al. (2023), both using the bubble method, reported rates of nitrogen fixation close to  $20 \text{ nmol N L}^{-1} \text{d}^{-1}$  around 8° N in November and May, respectively. These are consistent with our findings at 10° N in both cruises. Additionally, Voss et al. (2004) also found rates of nitrogen fixation close to  $70 \text{ nmol N L}^{-1} \text{d}^{-1}$  at two locations (8.2° N 25° W, and close to the coast of Africa at 10.4° N 16.8° W). Again, it is important to note that the highest rates reported to date have been found with our methodology ( $^{15}\text{N}_2$  bubble addition) rather than the dissolution method. Therefore, our findings in the Guinea Dome show unequivocally with direct in situ measurements the relevance of nitrogen fixation in this region of the Atlantic Ocean. This was recently hypothesized by Marshall et al. (2022), after finding an imprint of nitrogen fixation in the signatures of stable isotopes of nitrogen in nitrate in the Angola Gyre, which is an analog to the Guinea Dome in the south Atlantic Ocean. However, as we mentioned above, our increased spatial resolution also shows an unexpected patchiness of the system with relatively high rates that could have been missed with the usual spatial resolution of 3 to 4 degrees typical of most oceanographic surveys. This can be seen in the region between 8° and 15° N at 23° W in Fig. 6, where most of the rates in the literature are lower than ours. Contrastingly, our nitrogen fixation rates in the Equatorial band are not substantially higher than rates measured in fall or spring (Fig. 6), and lower than those reported by Subramaniam et al. (2013) during active boreal summer upwelling in the Equatorial Atlantic Ocean (e.g., the high rate at 2.5° N 23° W in Fig. 6 Bubble method panel). Therefore, our initial hypothesis (i.e., the low N:P ratio waters, resulting from residual phosphorus in aged upwelled waters, enhances nitrogen fixation in boreal summer relative to other seasons) remains unresolved probably due to the fact that we sampled too late at the end of the upwelling season.

In conclusion, *Trichodesmium* is present, and large colonies ( $> 500 \mu\text{m}$ ) can be found at the end of boreal summer in the Guinea Dome region, actively fixing nitrogen with relatively high rates (up to  $31 \text{ nmol N L}^{-1} \text{d}^{-1}$ ) that were not evident in previous studies. The Guinea Dome is a patchy region, with higher diazotrophic activities at the edges related to a likely sufficient supply of phosphorus and iron. In the Equatorial region, surface water presents a low dissolved inorganic nitrogen content but still

enough phosphorus for supporting what looks like a *Trichodesmium*-free community yielding moderate to low rates of nitrogen fixation ( $<4 \text{ nmol N L}^{-1} \text{ d}^{-1}$ ). Given that the timing of our cruises was at the end of the upwelling season, the results presented here bring to question the hypothesis put forward by Subramaniam et al. (2013) that residual phosphorus and iron can fuel significant nitrogen fixation as late as September. The impact on diazotrophy due to the synergy between dynamic and short temporal resolution physical processes in this region is still unknown and calls for further high-resolution studies.

**Acknowledgements** We would like to thank the captains, officers and crew of the RV Meteor for their skilled support at sea, which made our measurements possible; as well as the science parties of M119 and M130, who made a memorable journey. In addition, we would like to acknowledge the work of three anonymous reviewers and the handling editor, whose comments strengthen this manuscript.

**Author contributions** AF-C and AS conceived and designed the study. Research cruises were proposed and led by MD and PB, who provided hydrographic and zonal velocities. Nutrient data were provided by JPM, AS and EPA. DSH prepared and analyzed the modelled iron deposition. *Trichodesmium* colonies observed by the UVP5 were collected and analyzed by RK and HH. Incubation experiments were performed by AF-C. Isotope analysis were provided by JPM. Data analysis and the first draft of the manuscript was done by AF-C. All authors commented on previous versions of the manuscript and approved the final manuscript.

**Funding** Open Access funding enabled and organized by Projekt DEAL. The RV Meteor cruises were possible thanks to the financial support through the DFG for the “*Sonderforschungsbereich754: Climate-Biogeochemistry Interactions in the Tropical Ocean*”, and also through the BMBF-funded joint projects *NORDATLANTIK*, *RACE*, and *RACE II* (FKZ 03F0443B, 03F0651B, and 03F0729C) for M130. AF-C was funded by a Xunta de Galicia 2013 postdoctoral fellowship (POS-A/2013/142). RK acknowledges funding by the Heisenberg program of the German Science Foundation under project number 469175784. DSH acknowledges the support of NASA (grant IDS 80NSSC20K1674) and the Department of Energy (grant DE-SC0021302) and would like to acknowledge high-performance computing support from Cheyenne (<https://doi.org/10.5065/D6RX99HX>), provided by the National Center for Atmospheric Research’s Computational and Information Systems Laboratory, sponsored by the National Science Foundation. JPM acknowledges the support of NSF (grant OCE-1737078). RK and PB also acknowledge the support via the EU H2020 TRIATLAS project under grant agreement 817578. AS was supported by the Gordon and Betty Moore Foundation through Grant GBMF4886 to Columbia University and by NASA grant 80NSSC21K0439.

**Data availability** The CTD data is available in [doi.pangaea.de/10.1594/PANGAEA.860484](https://doi.org/10.1594/PANGAEA.860484) and [doi.pangaea.de/10.1594/PANGAEA.904367](https://doi.org/10.1594/PANGAEA.904367). The 75kHz ADCP can be accessed in [doi.pangaea.de/10.1594/PANGAEA.877375](https://doi.org/10.1594/PANGAEA.877375) and [doi.pangaea.de/10.1594/PANGAEA.904389](https://doi.org/10.1594/PANGAEA.904389). Nutrients are available in [doi.pangaea.de/10.1594/PANGAEA.934450](https://doi.org/10.1594/PANGAEA.934450) and [doi.pangaea.de/10.1594/PANGAEA.913986](https://doi.org/10.1594/PANGAEA.913986). The the rates of nitrogen fixation, stable isotopes of carbon and ancillary data are available in [https://doi.pangaea.de/10.1594/PANGAEA.962547](https://doi.org/10.1594/PANGAEA.962547) and [https://doi.pangaea.de/10.1594/PANGAEA.962553](https://doi.org/10.1594/PANGAEA.962553).

## Declarations

**Conflict of interest** The authors have no relevant financial or non-financial interests to disclose.

**Open Access** This article is licensed under a Creative Commons Attribution 4.0 International License, which permits use, sharing, adaptation, distribution and reproduction in any medium or format, as long as you give appropriate credit to the original author(s) and the source, provide a link to the Creative Commons licence, and indicate if changes were made. The images or other third party material in this article are included in the article’s Creative Commons licence, unless indicated otherwise in a credit line to the material. If material is not included in the article’s Creative Commons licence and your intended use is not permitted by statutory regulation or exceeds the permitted use, you will need to obtain permission directly from the copyright holder. To view a copy of this licence, visit <http://creativecommons.org/licenses/by/4.0/>.

## References

- Benavides M, Robidart J (2020) Bridging the spatiotemporal gap in diazotroph activity and diversity with high-resolution measurements. *Front Mar Sci*. <https://doi.org/10.3389/fmars.2020.568876>
- Benavides M, Voss M (2015) Five decades of  $\text{N}_2$  fixation research in the North Atlantic Ocean. *Front Mar Sci*. <https://doi.org/10.3389/fmars.2015.00040>
- Benavides M, Agawin NSR, Arístegui J et al (2011) Nitrogen fixation by *Trichodesmium* and small diazotrophs in the subtropical northeast Atlantic. *Aquat Microb Ecol* 65:43–53. <https://doi.org/10.3354/ame01534>
- Berman-Frank I, Cullen JT, Shaked Y et al (2001) Iron availability, cellular iron quotas, and nitrogen fixation in *Trichodesmium*. *Limnol Oceanogr* 46:1249–1260. <https://doi.org/10.4319/lo.2001.46.6.1249>
- Brandt P, Bange HW, Banyte D et al (2015) On the role of circulation and mixing in the ventilation of oxygen minimum zones with a focus on the eastern tropical North Atlantic. *Biogeosciences* 12:489–512. <https://doi.org/10.5194/bg-12-489-2015>
- Brandt P, Czeschel R, Schütte F et al (2017) ADCP current measurements (38 and 75 kHz) during METEOR cruise M119. <https://doi.org/10.1594/PANGAEA.877375>
- Breitbarth E, Oschlies A, LaRoche J (2007) Physiological constraints on the global distribution of *Trichodesmium*:



- effect of temperature on diazotrophy. *Biogeosciences* 4:53–61. <https://doi.org/10.5194/bg-4-53-2007>
- Capone DG, Hutchins DA (2013) Microbial biogeochemistry of coastal upwelling regimes in a changing ocean. *Nat Geosci* 6:711–717. <https://doi.org/10.1038/ngeo1916>
- Capone DG, Zehr JP, Paerl HW et al (1997) *Trichodesmium*, a globally significant marine cyanobacterium. *Science* (80) 276:1221–1229. <https://doi.org/10.1126/science.276.5316.1221>
- Carpenter EJ, Capone DG (1992) Nitrogen fixation in *Trichodesmium* blooms. In: Carpenter EJ, Capone DG, Rueter JG (eds) *Marine pelagic cyanobacteria*. Springer, Dordrecht, pp 211–217
- Carpenter EJ, Harvey HR, Fry B, Capone DG (1997) Biogeochemical tracers of the marine cyanobacterium *Trichodesmium*. *Deep Res Part I Oceanogr Res Pap* 44:27–38. [https://doi.org/10.1016/s0967-0637\(96\)00091-x](https://doi.org/10.1016/s0967-0637(96)00091-x)
- Carpenter EJ, Subramaniam A, Capone DG (2004) Biomass and primary productivity of the cyanobacterium *Trichodesmium* spp. in the tropical N Atlantic ocean. *Deep Sea Res Part I Oceanogr Res Pap* 51:173–203. <https://doi.org/10.1016/j.dsr.2003.10.006>
- Chanton J, Lewis FG (2002) Examination of coupling between primary and secondary production in a river-dominated estuary: Apalachicola Bay, Florida, USA. *Limnol Oceanogr* 47:683–697
- Chasar LC, Chanton JP, Koenig CC, Coleman FC (2005) Evaluating the effect of environmental disturbance on the trophic structure of Florida Bay, USA: multiple stable isotope analyses of contemporary and historical specimens. *Limnol Oceanogr* 50:1059–1072
- Christiansen S, Hoving H-J, Schütte F et al (2018) Particulate matter flux interception in oceanic mesoscale eddies by the polychaete *Poecobius* sp. *Limnol Oceanogr* 63:2093–2109. <https://doi.org/10.1002/lno.10926>
- Conway TM, Hamilton DS, Shelley RU et al (2019) Tracing and constraining anthropogenic aerosol iron fluxes to the North Atlantic Ocean using iron isotopes. *Nat Commun* 10:2628. <https://doi.org/10.1038/s41467-019-10457-w>
- Dengler M, Krahnmann G (2019) Physical oceanography (CTD) during METEOR cruise M130. <https://doi.org/10.1594/PANGAEA.904367>
- Dengler M, Czeschel R, Krahnmann G (2019) ADCP current measurements (38 and 75 kHz) during METEOR cruise M130. <https://doi.org/10.1594/PANGAEA.904389>
- Doi T, Tozuka T, Yamagata T (2009) Interannual variability of the Guinea Dome and its possible link with the Atlantic Meridional Mode. *Clim Dyn* 33:985–998. <https://doi.org/10.1007/s00382-009-0574-z>
- Fernández A, Mourriño-Carballido B, Bode A et al (2010) Latitudinal distribution of *Trichodesmium* spp. and N-2 fixation in the Atlantic Ocean. *Biogeosciences* 7:3167–3176. <https://doi.org/10.5194/bg-7-3167-2010>
- Fernandez C, González ML, Muñoz C et al (2015) Temporal and spatial variability of biological nitrogen fixation off the upwelling system of central Chile (35–38.5° S). *J Geophys Res Ocean* 120:3330–3349. <https://doi.org/10.1002/2014JC010410>
- Fischer J, Brandt P, Dengler M et al (2003) Surveying the upper ocean with the ocean surveyor: a new phased array doppler current profiler. *J Atmos Ocean Technol* 20:742–751. [https://doi.org/10.1175/1520-0426\(2003\)20%3c742:STUOWT%3e2.0.CO;2](https://doi.org/10.1175/1520-0426(2003)20%3c742:STUOWT%3e2.0.CO;2)
- Fong AA, Karl DM, Lukas R et al (2008) Nitrogen fixation in an anticyclonic eddy in the oligotrophic North Pacific Ocean. *ISME J* 2:663–676. <https://doi.org/10.1038/ismej.2008.22>
- Fonseca-Batista D, Dehairs F, Riou V et al (2017) Nitrogen fixation in the eastern Atlantic reaches similar levels in the Southern and Northern Hemisphere. *J Geophys Res Ocean* 122:587–601. <https://doi.org/10.1002/2016JC012335>
- Goebel NL, Turk KA, Achilles KM et al (2010) Abundance and distribution of major groups of diazotrophic cyanobacteria and their potential contribution to N(2) fixation in the tropical Atlantic Ocean. *Env Microbiol* 12:3272–3289. <https://doi.org/10.1111/j.1462-2920.2010.02303.x>
- Gómez-Rubio V (2017) ggplot2: elegant graphics for data analysis (2nd Edition). *J Stat Softw* 77:23. <https://doi.org/10.18637/jss.v077.b02>
- Grodsky SA, Carton JA, McClain CR (2008) Variability of upwelling and chlorophyll in the equatorial Atlantic. *Geophys Res Lett* 35:1–6. <https://doi.org/10.1029/2007GL032466>
- Grosskopf T, Mohr W, Baustian T et al (2012) Doubling of marine dinitrogen-fixation rates based on direct measurements. *Nature* 488:361–364. <https://doi.org/10.1038/nature11338>
- Gruber N (2004) The dynamics of the marine nitrogen cycle and its influence on atmospheric CO<sub>2</sub> variations BT—the ocean carbon cycle and climate. In: Follows M, Oguz T (eds). Springer Netherlands, Dordrecht, pp 97–148
- Gruber N (2008) Chapter 1: The marine nitrogen cycle: overview and challenges. In: Capone DG, Bronk DA, Mulholland MR, Carpenter EJB-T-N in the ME Second E (eds). Academic Press, San Diego, pp 1–50
- Hahn J, Brandt P, Schmidt S, Krahnmann G (2017) Decadal oxygen change in the eastern tropical North Atlantic. *Ocean Sci* 13:551–576. <https://doi.org/10.5194/os-13-551-2017>
- Hamilton DS, Scanza RA, Feng Y et al (2019) Improved methodologies for Earth system modelling of atmospheric soluble iron and observation comparisons using the Mechanism of Intermediate complexity for Modelling Iron (MIMI v1.0). *Geosci Model Dev* 12:3835–3862. <https://doi.org/10.5194/gmd-12-3835-2019>
- Hamilton DS, Scanza RA, Rathod SD et al (2020) Recent (1980 to 2015) trends and variability in daily-to-interannual soluble iron deposition from dust, fire, and anthropogenic sources. *Geophys Res Lett* 47:e2020GL089688. <https://doi.org/10.1029/2020GL089688>
- Hansen HP, Koroleff F (1999) Determination of nutrients. *Methods Seawater Anal* 159–228. <https://doi.org/10.1002/9783527613984.ch10>
- Hansman RL, Sessions AL (2016) Measuring the in situ carbon isotopic composition of distinct marine plankton populations sorted by flow cytometry. *Limnol Oceanogr Methods* 14:87–99. <https://doi.org/10.1002/lom3.10073>

- Held NA, Waterbury JB, Webb EA et al (2022) Dynamic diel proteome and daytime nitrogenase activity supports buoyancy in the cyanobacterium *Trichodesmium*. *Nat Microbiol* 7:300–311. <https://doi.org/10.1038/s41564-021-01028-1>
- Hummels R, Dengler M, Brandt P, Schlundt M (2014) Diapycnal heat flux and mixed layer heat budget within the Atlantic cold tongue. *Clim Dyn* 43:3179–3199. <https://doi.org/10.1007/s00382-014-2339-6>
- Hummels R, Dengler M, Rath W et al (2020) Surface cooling caused by rare but intense near-inertial wave induced mixing in the tropical Atlantic. *Nat Commun* 11:3829. <https://doi.org/10.1038/s41467-020-17601-x>
- Ibáñez JSP, Flores Montes M, Lefèvre N (2022) Evidence for enhanced primary production driving significant CO<sub>2</sub> drawdown associated with the Atlantic ITCZ. *Sci Total Environ* 838:156592. <https://doi.org/10.1016/j.scitotenv.2022.156592>
- Jayakumar A, Al-Rshaidat MM, Ward BB, Mulholland MR (2012) Diversity, distribution, and expression of diazotroph nifH genes in oxygen-deficient waters of the Arabian Sea. *FEMS Microbiol Ecol* 82:597–606. <https://doi.org/10.1111/j.1574-6941.2012.01430.x>
- Kara AB, Rochford PA, Hurlburt HE (2000) An optimal definition for ocean mixed layer depth. *J Geophys Res Ocean*. <https://doi.org/10.1029/2000JC900072>
- Karl D, Michaels A, Bergman B et al (2002) Dinitrogen fixation in the world's oceans. *Biogeochemistry* 57–58:47–98. <https://doi.org/10.1023/A:1015798105851>
- Kassambara A (2018) ggpubr: “ggplot2” Based Publication Ready Plots. R package version 0.2. <https://CRAN.R-project.org/package=ggpubr>. <https://CRAN.R-project.org/package=ggpubr>
- Kelley D (2011) Package “oce”: analysis of oceanographic data. R Packag.
- Kok JF (2011) A scaling theory for the size distribution of emitted dust aerosols suggests climate models underestimate the size of the global dust cycle. *Proc Natl Acad Sci* 108:1016–1021. <https://doi.org/10.1073/pnas.1014798108>
- Kok JF, Mahowald NM, Fratini G et al (2014) An improved dust emission model—part 1: model description and comparison against measurements. *Atmos Chem Phys* 14:13023–13041. <https://doi.org/10.5194/acp-14-13023-2014>
- Kok JF, Ridley DA, Zhou Q et al (2017) Smaller desert dust cooling effect estimated from analysis of dust size and abundance. *Nat Geosci* 10:274–278. <https://doi.org/10.1038/ngeo2912>
- Krahmann G, Arévalo-Martínez DL, Dale AW et al (2021) Climate-biogeochemistry interactions in the tropical ocean: data collection and legacy. *Front Mar Sci* 8:1270. <https://doi.org/10.3389/fmars.2021.723304>
- Krahmann G (2016) Physical oceanography during METEOR cruise M119. Suppl to Hahn, Johannes; Brand Peter; Schmidtko, Sunke; Krahmann, Gerd *Decad Oxyg Chang East Trop North Atl Ocean Sci* 13(4), 551–576. <https://doi.org/10.1594/PANGAEA.860484>
- Kustka A, Sañudo-Wilhelmy S, Carpenter EJ et al (2003) A revised estimate of the iron use efficiency of nitrogen fixation, with special reference to the marine cyanobacterium *Trichodesmium* spp. (Cyanophyta). *J Phycol* 39:12–25. <https://doi.org/10.1046/j.1529-8817.2003.01156.x>
- Landolfi A, Kähler P, Koeve W, Oschlies A (2018) Global marine N<sub>2</sub> fixation estimates: from observations to models. *Front Microbiol* 9:2112. <https://doi.org/10.3389/fmicb.2018.02112>
- Langlois RJ, LaRoche J, Raab PA (2005) Diazotrophic diversity and distribution in the tropical and subtropical Atlantic Ocean. *Appl Env Microbiol* 71:7910–7919. <https://doi.org/10.1128/AEM.71.12.7910-7919.2005>
- Li L, Mahowald N, Kok J et al (2022) Importance of different parameterization changes for the updated dust cycle modelling in the community atmosphere model (version 6.1). *Geosci Model Dev Discuss* 2022:1–49. <https://doi.org/10.5194/gmd-2022-31>
- Loescher CR, Bourbonnais A, Dekaezemaeker J et al (2016) N-2 fixation in eddies of the eastern tropical South Pacific Ocean. *Biogeosciences* 13:2889–2899. <https://doi.org/10.5194/bg-13-2889-2016>
- Longhurst A (1995) Seasonal cycles of pelagic production and consumption. *Prog Oceanogr* 36:77–167. [https://doi.org/10.1016/0079-6611\(95\)00015-1](https://doi.org/10.1016/0079-6611(95)00015-1)
- Luo YW, Doney SC, Anderson LA et al (2012) Database of diazotrophs in global ocean: abundance, biomass and nitrogen fixation rates. *Earth Syst Sci Data* 4:47–73. <https://doi.org/10.5194/essd-4-47-2012>
- Mahaffey C, Williams RG, Wolff GA et al (2003) Biogeochemical signatures of nitrogen fixation in the eastern North Atlantic. *Geophys Res Lett*. <https://doi.org/10.1029/2002gl016542>
- Marañón E, Holligan PM, Varela M et al (2000) Basin-scale variability of phytoplankton biomass, production and growth in the Atlantic Ocean. *Deep Sea Res Part I Oceanogr Res Pap* 47:825–857. [https://doi.org/10.1016/S0967-0637\(99\)00087-4](https://doi.org/10.1016/S0967-0637(99)00087-4)
- Marshall T, Granger J, Casciotti KL et al (2022) The Angola Gyre is a hotspot of dinitrogen fixation in the South Atlantic Ocean. *Commun Earth Environ* 3:151. <https://doi.org/10.1038/s43247-022-00474-x>
- Martínez-Pérez C, Mohr W, Löscher CR et al (2016) The small unicellular diazotrophic symbiont, UCYN-A, is a key player in the marine nitrogen cycle. *Nat Microbiol*. <https://doi.org/10.1038/nmicrobiol.2016.163>
- Mills MM, Ridame C, Davey M et al (2004) Iron and phosphorus co-limit nitrogen fixation in the eastern tropical North Atlantic. *Nature* 429:292–294. <https://doi.org/10.1038/nature02550>
- Mills MM, Turk-Kubo KA, van Dijken GL et al (2020) Unusual marine cyanobacteria/haptophyte symbiosis relies on N<sub>2</sub> fixation even in N-rich environments. *ISME J* 14:2395–2406. <https://doi.org/10.1038/s41396-020-0691-6>
- Mitchell TP, Wallace JM (1992) The annual cycle in equatorial convection and sea surface temperature. *J Clim* 5:1140–1156. [https://doi.org/10.1175/1520-0442\(1992\)005%3c1140:TACIEC%3e2.0.CO;2](https://doi.org/10.1175/1520-0442(1992)005%3c1140:TACIEC%3e2.0.CO;2)
- Mohr W, Grosskopf T, Wallace DW, LaRoche J (2010) Methodological underestimation of oceanic nitrogen fixation rates. *PLoS ONE* 5:e12583. <https://doi.org/10.1371/journal.pone.0012583>

- Montoya JP, Voss M, Kahler P, Capone DG (1996) A simple, high-precision, high-sensitivity tracer assay for N<sub>2</sub> fixation. *Appl Environ Microbiol* 62:986–993
- Montoya JP, Capone DG, Bronk DA et al (2008) Nitrogen stable isotopes in marine environments. In: *Nitrogen Marine Environment*, 2nd Edn, pp 1277–1302. <https://doi.org/10.1016/b978-0-12-372522-6.00029-3>
- Moore CM, Mills MM, Achterberg EP et al (2009) Large-scale distribution of Atlantic nitrogen fixation controlled by iron availability. *Nat Geosci* 2:867–871. <https://doi.org/10.1038/ngeo667>
- Moreira-Coello V, Mouriño-Carballido B, Marañón E et al (2017) Biological N<sub>2</sub> fixation in the upwelling region off NW Iberia: magnitude, relevance, and players. *Front Mar Sci*. <https://doi.org/10.3389/fmars.2017.00303>
- Mulholland MR, Bernhardt PW (2005) The effect of growth rate, phosphorus concentration, and temperature on N<sub>2</sub> fixation, carbon fixation, and nitrogen release in continuous cultures of *Trichodesmium* IMS101. *Limnol Oceanogr* 50:839–849. <https://doi.org/10.4319/lo.2005.50.3.0839>
- Mulholland MR, Bernhardt PW, Heil CA et al (2006) Nitrogen fixation and release of fixed nitrogen by *Trichodesmium* spp. in the Gulf of Mexico. *Limnol Oceanogr* 51:1762–1776. <https://doi.org/10.4319/lo.2006.51.4.1762>
- Pancost RD, Freeman KH, Wakeham SG, Robertson CY (1997) Controls on carbon isotope fractionation by diatoms in the Peru upwelling region. *Geochim Cosmochim Acta* 61:4983–4991. [https://doi.org/10.1016/S0016-7037\(97\)00351-7](https://doi.org/10.1016/S0016-7037(97)00351-7)
- Picheral M, Guidi L, Stemmann L et al (2010) The underwater vision profiler 5: an advanced instrument for high spatial resolution studies of particle size spectra and zooplankton. *Limnol Oceanogr Methods* 8:462–473. <https://doi.org/10.4319/lom.2010.8.462>
- Picheral M, Colin S, Irisson JO (2017) EcoTaxa, a tool for the taxonomic classification of images. <https://ecotaxa.obs-vlfr.fr/explore/>
- Rathod SD, Hamilton DS, Mahowald NM et al (2020) A Mineralogy-based anthropogenic combustion-iron emission inventory. *J Geophys Res Atmos* 125:e2019JD032114. <https://doi.org/10.1029/2019JD032114>
- Rees AP, Robinson C, Smyth T et al (2015) 20 years of the Atlantic meridional transect: AMT. *Limnol Oceanogr Bull*. <https://doi.org/10.1002/lob.10069>
- Rijkenberg MJA, Langlois RJ, Mills MM et al (2011) Environmental forcing of nitrogen fixation in the Eastern tropical and sub-tropical North Atlantic Ocean. *PLoS ONE* 6:e28989. <https://doi.org/10.1371/journal.pone.0028989>
- Rijkenberg MJA, Steigenger S, Powell CF et al (2012) Fluxes and distribution of dissolved iron in the eastern (sub-) tropical North Atlantic Ocean. *Global Biogeochem Cycles*. <https://doi.org/10.1029/2011GB004264>
- Rstudio T (2020) RStudio: Integrated Development for R. Rstudio Team, PBC, Boston, MA. <http://www.rstudio.com/>
- Sandel V, Kiko R, Brandt P et al (2015) Nitrogen fuelling of the pelagic food web of the tropical Atlantic. *PLoS ONE* 10:e0131258. <https://doi.org/10.1371/journal.pone.0131258>
- Scanza RA, Mahowald N, Ghan S et al (2015) Modeling dust as component minerals in the community atmosphere model: development of framework and impact on radiative forcing. *Atmos Chem Phys* 15:537–561. <https://doi.org/10.5194/acp-15-537-2015>
- Schlosser C, Klar JK, Wake BD et al (2014) Seasonal ITCZ migration dynamically controls the location of the (sub) tropical Atlantic biogeochemical divide. *Proc Natl Acad Sci* 111:1438LP – 1442. <https://doi.org/10.1073/pnas.1318670111>
- Schütte F, Brandt P, Karstensen J (2016) Occurrence and characteristics of mesoscale eddies in the tropical northeastern Atlantic Ocean. *Ocean Sci* 12:663–685. <https://doi.org/10.5194/os-12-663-2016>
- Shao Z, Xu Y, Wang H et al (2023) Global oceanic diazotroph database version 2 and elevated estimate of global oceanic N<sub>2</sub> fixation. *Earth Syst Sci Data* 15:3673–3709. <https://doi.org/10.5194/essd-15-3673-2023>
- Shiozaki T, Kodama T, Furuya K (2014) Large-scale impact of the island mass effect through nitrogen fixation in the western South Pacific Ocean. *Geophys Res Lett* 41:2907–2913. <https://doi.org/10.1002/2014GL059835>
- Siedler G, Zangenberg N, Onken R, Morlière A (1992) Seasonal changes in the tropical Atlantic circulation: observation and simulation of the Guinea Dome. *J Geophys Res Ocean* 97:703–715. <https://doi.org/10.1029/91JC02501>
- Singh A, Bach LT, Fischer T et al (2017) Niche construction by non-diazotrophs for N<sub>2</sub> fixers in the eastern tropical North Atlantic Ocean. *Geophys Res Lett*. <https://doi.org/10.1002/2017GL074218>
- Sloyan BM, Wanninkhof R, Kramp M et al (2019) The global ocean ship-based hydrographic investigations program (GO-SHIP): a platform for integrated multidisciplinary ocean science. *Front Mar Sci* 6:445
- Sohm JA, Hilton JA, Noble AE et al (2011) Nitrogen fixation in the South Atlantic Gyre and the Benguela upwelling system. *Geophys Res Lett* 38:1–6. <https://doi.org/10.1029/2011GL048315>
- Stal LJ (2009) Is the distribution of nitrogen-fixing cyanobacteria in the oceans related to temperature? *Env Microbiol* 11:1632–1645. <https://doi.org/10.1111/j.1758-2229.2009.00016.x>
- Subramaniam A, Mahaffey C, Johns W, Mahowald N (2013) Equatorial upwelling enhances nitrogen fixation in the Atlantic Ocean. *Geophys Res Lett*. <https://doi.org/10.1002/grl.50250>
- Subramaniam A, Krahnemann G (2021) Hydrochemistry of water samples during METEOR cruise M119. <https://doi.org/10.1594/PANGAEA.934450>
- Tang W, Li Z, Cassar N (2019a) Machine learning estimates of global marine nitrogen fixation. *J Geophys Res Biogeosciences* 124:717–730. <https://doi.org/10.1029/2018JG004828>
- Tang W, Wang S, Fonseca-Batista D et al (2019b) Revisiting the distribution of oceanic N<sub>2</sub> fixation and estimating diazotrophic contribution to marine production. *Nat Commun* 10:831. <https://doi.org/10.1038/s41467-019-08640-0>

- Tanhua T (2021) Hydrochemistry of water samples during METEOR cruise M145. <https://doi.org/10.1594/PANGAEA.934461>
- Tyrrell T, Marañón E, Poulton AJ et al (2003) Large-scale latitudinal distribution of *Trichodesmium* spp. in the Atlantic Ocean. *J Plankton Res* 25:405–416. <https://doi.org/10.1093/plankt/25.4.405>
- Villareal TA, Carpenter EJ (1990) Diel buoyancy regulation in the marine diazotrophic cyanobacterium *Trichodesmium thiebautii*. *Limnol Oceanogr* 35:1832–1837. <https://doi.org/10.4319/lo.1990.35.8.1832>
- Vitousek PM, Howarth RW (1991) Nitrogen limitation on land and in the sea: how can it occur. *Biogeochemistry* 13:87–115
- von Schuckmann K, Brandt P, Eden C (2008) Generation of tropical instability waves in the Atlantic Ocean. *J Geophys Res Ocean*. <https://doi.org/10.1029/2007JC004712>
- Voss M, Croot P, Lochte K et al (2004) Patterns of nitrogen fixation along 10° N in the tropical Atlantic. *Geophys Res Lett*. <https://doi.org/10.1029/2004GL020127>
- Wannicke N, Benavides M, Dalsgaard T et al (2018) New perspectives on nitrogen fixation measurements using  $^{15}\text{N}_2$  gas. *Front Mar Sci* 5:1–10. <https://doi.org/10.3389/fmars.2018.00120>
- Wasmund N, Struck U, Hansen A et al (2015) Missing nitrogen fixation in the Benguela region. *Deep Res Part I Oceanogr Res Pap* 106:30–41. <https://doi.org/10.1016/j.dsr.2015.10.007>
- Weber ED, McClatchie S (2009) Rcalcofi: analysis and visualization of CalCOFI data in R. *Calif Coop Ocean Fish Investig Rep* 50:178
- Weiss RF (1970) The solubility of nitrogen, oxygen and argon in water and seawater. *Deep Sea Res Oceanogr Abstr* 17:721–735. [https://doi.org/10.1016/0011-7471\(70\)90037-9](https://doi.org/10.1016/0011-7471(70)90037-9)
- Wen Z, Lin W, Shen R et al (2017) Nitrogen fixation in two coastal upwelling regions of the Taiwan Strait. *Sci Rep* 7:17601. <https://doi.org/10.1038/s41598-017-18006-5>
- White AE, Granger J, Selden C et al (2020) A critical review of the  $^{15}\text{N}_2$  tracer method to measure diazotrophic production in pelagic ecosystems. *Limnol Oceanogr Methods* 18:129–147. <https://doi.org/10.1002/lom3.10353>
- Wiedinmyer C, Akagi SK, Yokelson RJ et al (2011) The Fire INventory from NCAR (FINN): a high resolution global model to estimate the emissions from open burning. *Geosci Model Dev* 4:625–641. <https://doi.org/10.5194/gmd-4-625-2011>
- Zehr JP, Bombar D (2015) Marine nitrogen fixation: organisms, significance, enigmas, and future directions. In: de Bruijn FJ (ed) *Biological Nitrogen Fixation*. <https://doi.org/10.1002/9781119053095.ch84>
- Zehr JP, Capone DG (2020) Changing perspectives in marine nitrogen fixation. *Science* (80) 368:eaay9514. <https://doi.org/10.1126/science.aay9514>
- Zender CS, Bian H, Newman D (2003) Mineral dust entrainment and deposition (DEAD) model: description and 1990s dust climatology. *J Geophys Res Atmos* 108:2. <https://doi.org/10.1029/2002JD002775>

**Publisher's Note** Springer Nature remains neutral with regard to jurisdictional claims in published maps and institutional affiliations.